# Performance Analysis of Timer-Based Burst Assembly with Slotted Scheduling for Optical Burst Switching Networks

Takuji TACHIBANA and Shoji KASAHARA

Graduate School of Information Science,
Nara Institute of Science and Technology
Takayama 8916-5, Ikoma, Nara 630-0192, Japan
Email: {takuji-t, kasahara}@is.naist.jp
Tel: +81–743–72–5351, Fax: +81–743–72–5359

**Abstract**

In this paper, we analyze the performance of a timer-based burst assembly for optical burst switching (OBS) networks. In our analytical model, an ingress edge node has multiple buffers where IP packets are stored depending on their egress edge nodes, and bursts are assembled at the buffers in round-robin manner. Moreover, bursts are transmitted in accordance with slotted scheduling where each burst transmission starts at slot boundary. We construct a loss model with two independent arrival streams, and explicitly derive the burst loss probability, burst throughput, and data throughput. In numerical examples, we show the effectiveness of our analysis in comparison with the Erlang loss system. It is shown that our model is quite useful for an OBS network with large number of input and output links. We also evaluate the performance of the timer-based burst assembly for uni-directional ring and mesh-torus networks with simulation, and discuss the effectiveness of our analysis for both networks.

**Index Terms:** Optical burst switching, Timer-based burst assembly, Queueing model, Erlang loss system, Slotted transmission scheduling

## I. Introduction

Optical burst switching (OBS) has received considerable attention as one of the most promising technologies for supporting the next-generation Internet over wavelength division multiplexing (WDM) network [2], [6], [15], [23], [27], [28]. In OBS networks, multiple IP packets are assembled into a burst with variable length at an ingress edge node and is transmitted to its egress one. A burst is pure payload and has the associated control packet which contains control information such as burst length and routing information [7], [25].

In order to reduce signaling delay, a source node starts burst transmission without receiving any acknowledgement from its egress edge node (one-way reservation). For the one-way reservation, several signaling protocols have been proposed with regard to the reservation period of a wavelength for the burst transmission [3], [16], [17].

In Just-Enough-Time (JET) signaling protocol, a source node sends a control packet and then sends the corresponding burst after some offset time [27], [28]. Using extra information to better predict the start and end of the burst, a wavelength is reserved efficiently to transmit the burst. Therefore, the JET protocol will achieve a better performance than other signaling protocols [16].

Burst assembly is also an important issue for the OBS and several burst assembly techniques have been proposed. Most of the techniques are classified into threshold-based and timer-based burst assemblies. [20] proposed a threshold-based burst assembly technique in which a threshold is used in order to limit the maximum number of packets within a burst. With this burst assembly, bursts with the same length are frequently transmitted over the OBS network.

In [6], a timer-based burst assembly technique called the *Fixed-Time-Min-Length burst assembly algorithm* was proposed. In this technique, a timer is started at the arrival time of the first packet and a burst is assembled when the timer reaches a pre-specified timeout value. If the amount of IP packets for the burst is too small, it is assembled with padding the null data. This burst assembly technique creates bursts with variable length but provides an upper bound on delay due to the timeout value. [29] reported that the distribution of burst length approaches to a Gaussian distribution with zero variance when the timeout value becomes large.

[25] proposed the timer-based burst assembly in which both the timeout value and the maximum burst size are taken into consideration. [21] developed the [25]'s scheme into the one which provides a QoS guarantee. [1] proposed a timer-based burst assembly algorithm focusing on the TCP congestion control. In this method, the timeout value and the minimum burst size are adapted to TCP flows. [11] considered the DiffServ-based burst assembly scheme where each burst assembly time is adapted to the actual traffic arrival rate and the QoS requirement.

The assembled burst is sent into the OBS network after some offset time which is calculated according to burst scheduling [21]. In the first-come first-served (FCFS) scheduling, bursts are transmitted in their assembling order. In the priority queueing (PQ), a burst with low priority is sent to an output port only if there is no burst with high priority. In the weighted round-robin (WRR), each prioritized burst queue is served in a round-robin order and the number of bursts sent in each round depends on the weight assigned by the policy. In the waiting time priority (WTP), a scheduler transmits the burst with the longest waiting time to the OBS network.

As for the performance issue of the JET signaling protocol in the OBS network, several studies have appeared in the literature. In those studies, the Erlang loss system, i.e., the M/M/$c$/$c$ queueing model, plays an important role for the analysis of burst loss probability. For example, the burst loss probability for the OBS node without fiber delay lines (FDLs) was analyzed using the M/M/$c$/$c$ in [4], [19], [22], and [28]. In [26], a probabilistic preemption scheme for service differentiation in OBS networks was analyzed with a multi-dimensional Markov chain. As for the case where the OBS node has FDLs, an M/M/$c$/$K$ queueing model is utilized for the analysis of the burst loss probability [5], [12], [28].

[8] discussed the influence of self-similar traffic on assembled burst traffic in OBS core nodes and showed that a Poisson process can be assumed for the burst arrival process in the time-scale of burst blocking. It is well known that the burst size distribution significantly depends on the burst assembly technique. For example, the burst size distribution approaches to deterministic when the burst assembly is timer-based [8], [29]. [14] analyzed the blocking time distribution for bursts and investigated the effect of three burst-size distributions; the Pareto, Gaussian and exponential ones. However, to the best of our knowledge, the performance analysis in which both the burst assembly technique and burst transmission scheduling are taken into consideration has not been studied yet.

In this paper, we analyze the performance of the timer-based burst assembly at an edge OBS node without FDLs. A burst is assembled in a round-robin manner, and with the JET signaling protocol, assembled bursts are transmitted into the OBS network at multiples of some fixed interval. In [18], we modeled the edge node as a loss model with deterministic and Poisson arrivals, assuming that assembled bursts are transmitted at fixed intervals from scheduler. In this paper, we extend the model to the one with geometric and Poisson arrivals, and explicitly derive the burst loss probability, burst throughput, and data throughput. We also investigate those performance measures for uni-directional ring and mesh-torus networks by simulation, and discuss the effectiveness of our analysis

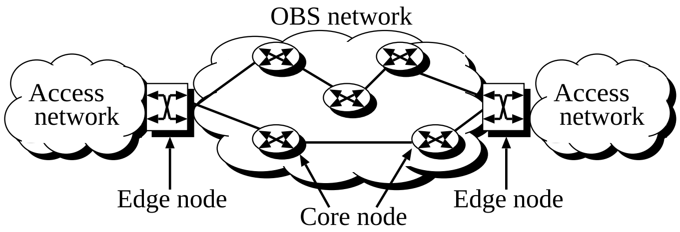


Fig. 1. OBS network.

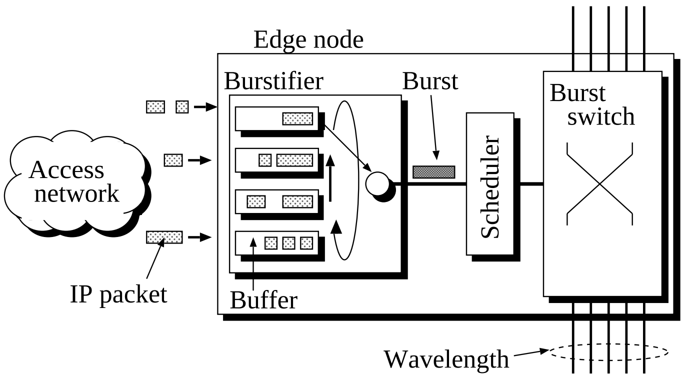


Fig. 2. Round-robin burst assembly.

in comparison with the Erlang loss model and simulation.

The rest of the paper is organized as follows. Section II presents the timer-based burst assembly and burst transmission scheduling, and in Section III, we describe our analytical model for an edge node. In section IV, we present the performance analysis of the model in detail and numerical examples are shown in Section V. Finally, conclusions are presented in Section VI.

## II. Timer-based burst assembly and slotted transmission scheduling

The OBS network considered in the paper consists of edge and core nodes, as shown in Fig. 1. An ingress edge node consists of a burstifier, a scheduler, and a burst switch (see Fig. 2). The burstifier has $L$ buffers, and IP packets arriving from its access network are stored in the buffers corresponding to their egress edge nodes.

In our scenario, bursts are assembled with multiple IP packets stored in each buffer, and each burst assembly is processed in round-robin fashion. The burst assembly processing time at each buffer is constant and equal to $T$. We define the cycle time of a round-robin process as the total processing time at the $L$ buffers and thus it is given by $LT$. Therefore, in each buffer, a burst is assembled with IP packets stored during the cycle time $LT$. Let $D$ denote the minimum burst size. If the amount of IP packets just before the assembly is smaller than $D$, padding is performed such that the resulting burst size is equal to $D$.

The scheduler sends the associated control packet to the egress edge node and then transmits the burst into the OBS network after some offset time. The scheduler sends control packets so that bursts depart from the scheduler at multiples of $T$ as shown in Fig. 3. In this figure, we assume that $L$ is equal to 4.

Let $B_i$ $(i = 1, \cdots, L)$ denote the burst assembled in the $i$th buffer and $C_i$ the control packet associated with $B_i$. We define $\Delta_i$ as the offset time for $B_i$. Let $\tau_i$ $(i = 1, \cdots, L-1)$ and $\tau_L$ denote

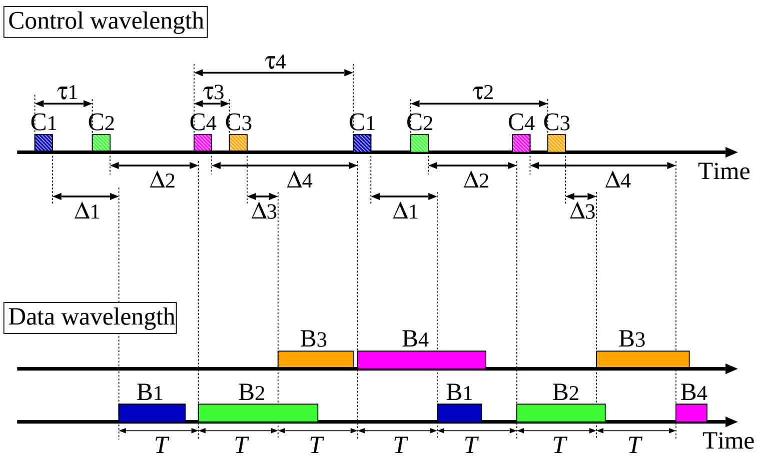


Fig. 3. Slotted transmission scheduling.

the transmission intervals between $C_i$ and $C_{i+1}$, and between $C_L$ and $C_1$, respectively.

When $\Delta_i$ and $\Delta_{i+1}$ $(i = 1, \cdots, L-1)$ satisfy

$$T + \Delta_i \geq \Delta_{i+1}, \tag{1}$$

$C_i$ is transmitted before $C_{i+1}$, and $\tau_i$ is set to $T + \Delta_i - \Delta_{i+1}$. On the other hand, when $\Delta_i$ and $\Delta_{i+1}$ $(i = 1, \cdots, L-1)$ satisfy

$$T + \Delta_i < \Delta_{i+1}, \tag{2}$$

$C_{i+1}$ is transmitted before $C_i$, and $\tau_i$ is set to $\Delta_{i+1} - T - \Delta_i$. In terms of $C_L$ and $C_1$, $i$ and $i+1$ in the above are replaced by $L$ and 1, respectively, and $\tau_L$ is determined in the same way.

Note that the order of control-packet transmissions are not always in sequence and that the transmission interval between consecutive control packets depends on the offset times of the corresponding bursts. However, the bursts are transmitted in sequence over the cycle time and each burst transmission starts at a multiple of $T$.

The assembled bursts are forwarded to the scheduler and then sent to the switch. The timer axis in the scheduler is segmented into a sequence of slots with size $T$, and it is assumed that the burst forwarding from the scheduler to the switch starts at the slot boundary if there exists at least one burst in the scheduler.

In the burst switch, wavelengths are used not only by bursts from the scheduler but also by those from other OBS nodes. When a control packet arrives at the OBS node and there are no available output wavelengths, the control packet fails in reserving a wavelength and the corresponding burst is lost.

## III. Analytical model

We focus on an ingress edge node for the performance analysis of the timer-based burst assembly. In the burstifier of the edge node, there are $L$ buffers and IP packets coming from the access network are stored in the buffers. (see Fig. 4.)

We assume that IP packets arrive at the edge node from the access network according to a Poisson process with rate $\lambda$ and that the egress edge nodes of the IP packets are equally likely. Because each IP packet is stored in the buffer corresponding to its egress node, IP packets arrive

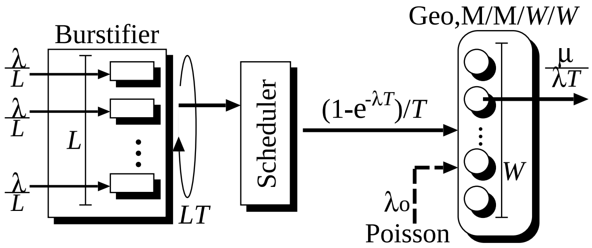


Fig. 4. Analytical model.

at each buffer according to a Poisson process with rate $\lambda/L$. Moreover, we assume that the mean length of an arriving IP packet is $M$ bits. When the transmission speed of a wavelength is $B$ bps, an IP packet is transmitted with the mean transmission time $1/\mu = M/B$.

The processing time of a burst assembly at each buffer is a fixed time equal to $T$. We assume that the buffer with no IP packet is served with the processing time $T$. Therefore, a burst is assembled with multiple IP packets which are stored during the cycle time $LT$. Hence the mean transmission time of a burst at the switch is given by $\lambda T/\mu = \lambda MT/B$. We assume that the transmission time of a burst is exponentially distributed with the mean $\lambda MT/B$ [1].

The assembled bursts are forwarded to the scheduler and then sent to the switch. The timer axis in the scheduler is segmented into a sequence of slots with size $T$, and it is assumed that the burst forwarding from the scheduler to the switch starts at the slot boundary if there exists at least one burst in the scheduler. Because the packet arrival process at each buffer is Poisson with parameter $\lambda/L$ and the cycle time is $LT$, the probability that there exists a burst in the scheduler at the slot boundary is given by $1 - e^{-\lambda T}$.

Note that the burst inter-departure time at the scheduler is geometrically distributed with a mean of $1/(1 - e^{-\lambda T})$ slots. That is, denoting A as the burst inter-departure time, we have

$$\Pr\{A = kT\} = (1 - e^{-\lambda T})e^{-(k-1)\lambda T}, \quad k \geq 1. \tag{3}$$

There are $W$ output wavelengths in the switch and two types of bursts are transmitted with the wavelengths; the bursts from the scheduler and those from the other edge nodes. We assume that the OBS network has many edge nodes and that each node's scheduler is not synchronized with other schedulers. If a large number of the burst arrival processes are independent and each burst arrival process contributes a small fraction to the load, the compound burst arrival process can be approximated by a Poisson process [10]. Following [10], we approximate the compound burst arrival process from the other nodes by a Poisson process with rate $\lambda_o$.

## IV. Performance analysis

From the assumptions in Section III, we have a $\mathrm{Geo}, \mathrm{M}/\mathrm{M}/W/W$ queueing model as shown in Fig. 4. In this section, we explicitly derive the burst loss probability, burst throughput, and data throughput for the $\mathrm{Geo}, \mathrm{M}/\mathrm{M}/W/W$ system. In the following, we assume that the system is in equilibrium.

[1] [29] reported that with the assumption of Poisson arrivals for IP packets, the distribution of burst length approaches to a deterministic distribution as the timeout value becomes large. In general, however, a multiserver queueing system whose service distribution is general is not analyzable expect for the Erlang loss system. For analytical simplicity, we assume the exponential distribution for the burst-transmission time.

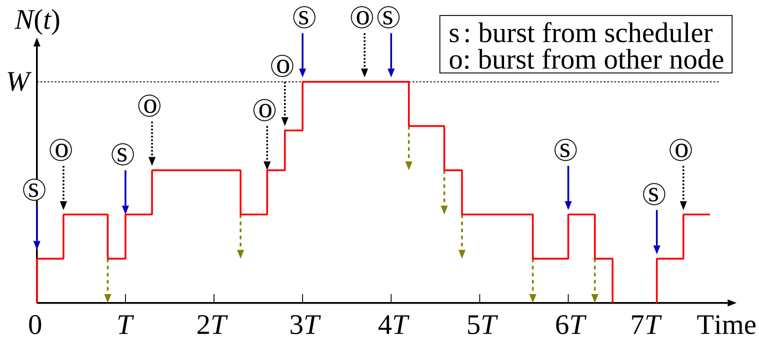


Fig. 5. Sample path for Geo,M/M/$W$/$W$ queueing model.

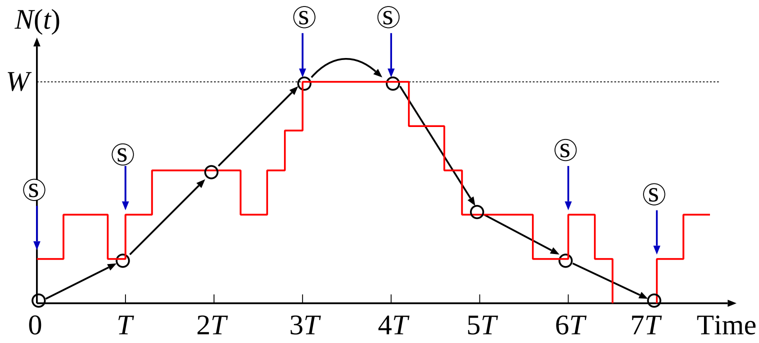


Fig. 6. Geometric arrivals in the sample path.

Let $N(t)$ denote the number of bursts being transmitted in the system at time $t$. Without loss of generality, we assume that the event of a burst arrival from the scheduler occurs at multiples of $T$. Fig. 5 shows the sample path of $N(t)$. In this figure, burst arrivals from the scheduler occur at multiples of $T$, while those from the other nodes occur at arbitrary points.

First, we focus on the system state just before the slot boundary (white circles in Fig. 6). We define the number of bursts in the system just before the $n$th slot as $N_n^- = N(nT^-)$ $(n = 0, 1, \cdots)$. With the assumptions of Poisson arrivals from the other nodes and the exponential transmission time, the process $\{N_n^- : n = 0, 1, \cdots\}$ is a discrete-time Markov chain. We define the steady state probability for the Markov chain as

$$q_k = \lim_{n\to\infty} P_r\{N_n^- = k\}, \;\; 0 \le k \le W. \tag{4}$$

To derive the transition probability of $q_k$, we consider the state transition between $N_n^-$ and $N_{n+1}^-$. Note that the state transition between $N_n^-$ and $N_{n+1}^-$ consists of two parts: one is the event of a burst arrival from the scheduler at $nT$ (the $n$th slot boundary), and the other is the transition from the state just after the $n$th slot boundary to the state just before the $n+1$st slot boundary. Note that the latter state transition is the same as an M/M/$W$/$W$ queueing model in which the arrival process is Poisson with rate $\lambda_o$ and the service time is exponentially distributed with the mean $\lambda T/\mu$. The state transition diagram for the M/M/$W$/$W$ queueing model is illustrated in Fig. 7. Let $\boldsymbol{Q}$ denote the infinitesimal generator of the M/M/$W$/$W$. $\boldsymbol{Q}$ is a $(W+1)\times(W+1)$ matrix

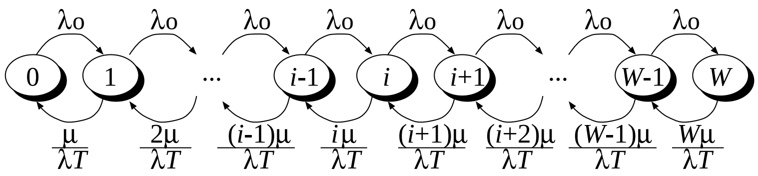


Fig. 7. State transition diagram.

whose $(i,j)$th element is given by

$$[\boldsymbol{Q}]_{ij} = \begin{cases} \lambda_o, & 1 \le i \le W,\ \ j=i+1, \\ -\left\{\lambda_o + \frac{(i-1)\mu}{\lambda T}\right\}, & 1 \le i \le W+1,\ \ j=i, \\ \frac{(i-1)\mu}{\lambda T}, & 2 \le i \le W+1,\ \ j=i-1, \\ 0, & \text{otherwise.} \end{cases} \tag{5}$$

For $s$ and $t$ $(0 \le s < t < T)$, we define $\boldsymbol{H}(s,t)$ as the M/M/$W$/$W$ state-transition probability matrix from the state at time $s$ to the state at time $t$. $\boldsymbol{H}(s,t)$ satisfies the forward Chapman-Kolmogorov equation

$$\frac{\partial \boldsymbol{H}(s,t)}{\partial t} = \boldsymbol{H}(s,t)\boldsymbol{Q}. \tag{6}$$

In the following, $\boldsymbol{H}(0,t) \equiv \boldsymbol{H}(t)$ and $\boldsymbol{I}$ is the identity matrix. With the initial condition $\boldsymbol{H}(0) = \boldsymbol{I}$ and (6), $\boldsymbol{H}(t)$ is given by $\boldsymbol{H}(t) = e^{\boldsymbol{Q}t}$.

Note that a burst arrival from the scheduler occurs with probability $1 - e^{-\lambda T}$. Therefore, the system state just after the $n$th slot boundary is $\min(N_n^- + 1, W)$ with probability $1 - e^{-\lambda T}$, or $N_n^-$ with probability $e^{-\lambda T}$. Since the slot size is $T$, the transition probabilities for $q_k$ are then given by

$$\begin{aligned} U_{ij} &\equiv P_r\{N_{n+1}^- = j | N_n^- = i\} \\ &= \begin{cases} (1-e^{-\lambda T})[\boldsymbol{H}(T)]_{i+1,j} + e^{-\lambda T}[\boldsymbol{H}(T)]_{i,j}, & 0 \le i \le W-1,\ \ 0 \le j \le W, \\ [\boldsymbol{H}(T)]_{W,j}, & i = W,\ \ 0 \le j \le W. \end{cases} \end{aligned} \tag{7}$$

With $\boldsymbol{U} = [U_{ij}]$, $\boldsymbol{q} = (q_0, \cdots, q_W)$, and $\boldsymbol{e} = (1, \cdots, 1)^T$, $\boldsymbol{q}$ is determined from the equilibrium equations $\boldsymbol{q} = \boldsymbol{q}\boldsymbol{U}$ and the normalizing condition $\boldsymbol{q}\boldsymbol{e} = 1$. Given that a burst arrival from the scheduler occurs, the burst is lost with probability $q_W$.

Next, we consider the steady-state probability at an arbitrary point defined as $p_k = \lim_{t\to\infty} P_r\{N(t) = k\}$. Note that $P_k$ is the same as the probability that the burst arrivals from the other nodes (Poisson arrivals, black circles in Fig. 8) find $k$ bursts in the system (Poisson arrivals see time averages, [24]). We define the $n$th cycle as the time interval $[nT, (n+1)T)$. From the assumptions in our analytical model, it is clear that the process $N(t)$ regenerates itself at $nT$ $(n = 0, 1, \cdots)$. With the renewal-reward theorem [24, p. 60], we have for $k = 0, 1, 2, \cdots$,

$$p_k = \lim_{t\to\infty} \frac{1}{t}\int_0^t \mathbf{1}_{\{N(t)=k\}} dt = \frac{1}{T}\int_0^{T^-} E\left[\mathbf{1}_{\{N(t)=k\}}\right] dt, \tag{8}$$

where $\mathbf{1}_{\{X\}}$ is the indicator function of event $X$. (8) implies that the steady state probability at an arbitrary time is equal to the time average of the number of bursts in the system over one cycle. Therefore, we consider the time average of $N(t)$ over one cycle.

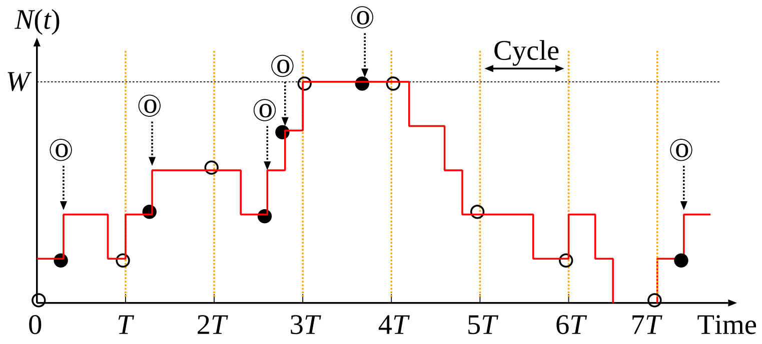


Fig. 8. Poisson arrivals in the sample path.

Let $\{r_k : k = 0, \cdots, W\}$ denote the state probability at the beginning of a cycle. With the steady state probability $q_k$, $r_k$ is given by the following equations.

$$r_k = \begin{cases} e^{-\lambda T} q_0, & k = 0, \\ (1 - e^{-\lambda T}) q_{k-1} + e^{-\lambda T} q_k, & 0 < k < W, \\ (1 - e^{-\lambda T}) q_{W-1} + q_W, & k = W. \end{cases} \tag{9}$$

Let $\boldsymbol{p} = (p_0, \cdots, p_W)$ and $\boldsymbol{r} = (r_0, \cdots, r_W)$. For $0 \le t < T$, we have

$$E\left[\mathbf{1}_{\{N(t)=k\}}\right] = \left[\boldsymbol{r} e^{\boldsymbol{Q}t}\right]_k, \tag{10}$$

where $[\boldsymbol{x}]_k$ denote the $k$th element of vector $\boldsymbol{x}$. Substituting (10) into (8), we obtain

$$\boldsymbol{p} = \frac{1}{T}\boldsymbol{r} \int_0^{T^-} e^{\boldsymbol{Q}t} dt = \frac{1}{T}\boldsymbol{r} \int_0^{T} e^{\boldsymbol{Q}t} dt = \frac{1}{T}\boldsymbol{r} \sum_{k=0}^{\infty} \frac{\boldsymbol{Q}^k T^{k+1}}{(k+1)!}, \tag{11}$$

where we use the continuity of $e^{\boldsymbol{Q}t}$ in the second equality.

In (11), $\boldsymbol{Q}$ is the infinitesimal generator of M/M/$W$/$W$ and hence $\boldsymbol{Q}$ is singular. Now we consider the matrix $\boldsymbol{e\pi} - \boldsymbol{Q}$ where $\boldsymbol{\pi}$ is the steady-state probability vector of M/M/$W$/$W$ such that $\boldsymbol{\pi Q} = \boldsymbol{0}$ and $\boldsymbol{\pi e} = 1$. Here, $\boldsymbol{e\pi} - \boldsymbol{Q}$ is nonsingular [13] and has an inverse matrix. In addition, $\boldsymbol{Q}$ and $\boldsymbol{\pi}$ satisfy the following equation

$$\boldsymbol{Q}(\boldsymbol{e\pi} - \boldsymbol{Q}) = -\boldsymbol{Q}^2. \tag{12}$$

Hence, we have

$$\boldsymbol{Q} = \boldsymbol{Q}^2(\boldsymbol{Q} - \boldsymbol{e\pi})^{-1}. \tag{13}$$

With (11) and (13), $\boldsymbol{p}$ is explicitly given by

$$\boldsymbol{p} = \frac{1}{T}\boldsymbol{r}\left\{\boldsymbol{I}T + (e^{\boldsymbol{Q}T} - \boldsymbol{I} - \boldsymbol{Q}T)(\boldsymbol{Q} - \boldsymbol{e\pi})^{-1}\right\}. \tag{14}$$

Because Poisson arrivals see time average (PASTA) [24], the loss probability for the bursts from the other nodes is given by $p_W$.

With $q_W$ and $p_W$, the burst loss probability $P_{loss}$ is given by the following equation.

$$P_{loss} = \frac{(1 - e^{-\lambda T}) q_W + \lambda_o T p_W}{1 - e^{-\lambda T} + \lambda_o T}. \tag{15}$$

The burst throughput defined as the number of transmitted bursts per unit of time, $T_{hr}^{(b)}$, is given by

$$T_{hr}^{(b)} = \frac{(1 - e^{-\lambda T})(1 - q_W)}{T} + \lambda_o(1 - p_W). \tag{16}$$

Finally, the data throughput defined as the amount of transmitted data (bits) per unit of time, $T_{hr}^{(d)}$, is derived as

$$T_{hr}^{(d)} = \lambda M \left\{(1 - e^{-\lambda T})(1 - q_W) + \lambda_o T(1 - p_W)\right\}. \tag{17}$$

## V. Numerical examples

In our numerical examples, we assume that the transmission speed of each output wavelength $B$ is 10 Gbps and that IP packets with the mean size of 1,250 bytes, i.e. $M = 10,000$ bits, arrive at the edge node from the access network. Thus, the mean transmission speed of an IP packet, $1/\mu$, is 1.0 $\mu$s and in the following, the unit of time is 1.0 $\mu$s. In addition, we set $\mu = 1.0$ and the minimum burst size $D$ is equal to 64 kbytes.

### *A. An edge node in OBS network*

In this subsection, we assume that the number of buffers $L$ is equal to 5. The burst loss probability, burst throughput [number of bursts/s], and data throughput [Gbps] are calculated by the analysis in the previous section and by simulation. The assumptions we made for the simulation are the same as the analysis, except that the IP packet size is constant and equal to 1,250 bytes. Note that the probability distribution of the resulting burst size is not an exponential one.

We also compare the analysis with the Erlang loss system which has been extensively used as a reference model for evaluating the loss performance in the literature [28]. For the Erlang loss system, the burst loss probability, burst throughput, and data throughput are given by

$$P_{loss}^{(Erlang)} = \frac{\{\lambda T(1/T + \lambda_o)/\mu\}^W/W!}{\sum_{k=0}^{W}\{\lambda T(1/T + \lambda_o)/\mu\}^k/k!}, \tag{18}$$

$$T_{hr}^{(b)(Erlang)} = (1/T + \lambda_o)\left\{1 - P_{loss}^{(Erlang)}\right\}, \tag{19}$$

$$T_{hr}^{(d)(Erlang)} = \lambda M T(1/T + \lambda_o)\left\{1 - P_{loss}^{(Erlang)}\right\}. \tag{20}$$

#### A.1 Impact of burst assembly processing time

First, we consider how the burst assembly processing time $T$ affects the burst loss probability, burst throughput, and data throughput. Here, we set $W = 32$ and $\lambda = 1.0$. $\lambda_o$ is determined so that the system utilization factor $\rho = \lambda(1 + \lambda_o T)/W\mu$ is unchanged.

Fig. 9 illustrates the loss probability against the burst-assembly processing time with $\rho = 0.4$, 0.5, 0.75, and 1.0, and Figs. 10 to 11 illustrate the burst and data throughputs, respectively. These results are calculated by our analysis and simulation. From these figures, we observe that the analytical and simulation results are almost the same in the case of large $\rho$ and that the discrepancy between these two results is small even when $\rho = 0.4$. Table I shows the results of the Geo,M/M/$W$/$W$, Erlang, and simulation in the case of small $T$. The table shows that if $T$ is large and the padding is not used, the result of Geo,M/M/$W$/$W$ is more close to that of the simulation than the Erlang loss model. These results validate the efficiency of the analysis under the above conditions.

Fig. 9 shows that the burst loss probability does not change as the burst assembly processing time becomes large. When the burst assembly processing time is large, large bursts are assembled

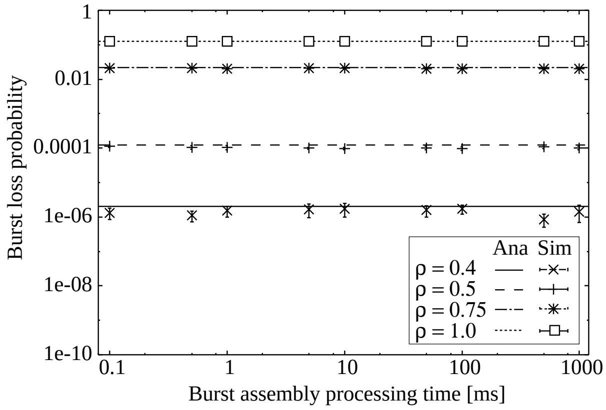


Fig. 9. Burst loss probability vs. burst assembly processing time.

TABLE I
COMPARISON OF RESULTS OF GEO,M/M/$W$/$W$, ERLANG, AND SIMULATION IN THE CASE OF $\rho = 0.5$.

| $T$ [ms] | Metrics | Erlang | Geo,M/M/$W$/$W$ | Simulation |
|---|---|---|---|---|
| 0.05 | $P_{loss}$ | 1.45e-04 | 1.22e-04 | (3.46±0.12)e-04 |
| | $T_{hr}^{(b)}$ | 319.95 | 319.96 | 319.87±0.14 |
| | $T_{hr}^{(d)}$ | 159.97 | 159.98 | 159.93e±0.07 |
| 0.1 | $P_{loss}$ | 1.45e-04 | 1.22e-04 | (1.13±0.09)e-04 |
| | $T_{hr}^{(b)}$ | 159.97 | 159.98 | 159.95±0.09 |
| | $T_{hr}^{(d)}$ | 159.97 | 159.98 | 159.95±0.09 |
| 0.5 | $P_{loss}$ | 1.45e-04 | 1.22e-04 | (1.16±0.08)e-04 |
| | $T_{hr}^{(b)}$ | 31.99 | 31.98 | 31.99±0.03 |
| | $T_{hr}^{(d)}$ | 159.97 | 159.98 | 159.99±0.02 |

at the edge node. However, the interval between consecutive burst transmissions also becomes large. Therefore, the burst assembly processing time does not affect the burst loss probability for the timer-based burst assembly. In Fig. 9, we also find that the burst loss probability becomes large as the system utilization factor $\rho$ increases.

From Fig. 10, we observe that the burst throughput becomes small as the burst assembly processing time increases. This is because the increase of the burst assembly processing time causes a large burst-transmission interval. As a result, the burst-transmission delay becomes large and the number of transmitted bursts per unit of time becomes small. The burst throughput also decreases as the system utilization factor becomes small, however, the impact of the system utilization factor on the burst throughput is smaller than that of the burst assembly processing time. On the other hand, in Fig. 11, the data throughput does not change as the burst assembly processing time becomes large.

From these observations, the burst loss probability and data throughput are insensitive to the burst assembly processing time while the burst throughput is sensitive to the burst assembly processing time. Note that the decrease of the burst throughput implies the increase of the burst-transmission delay.

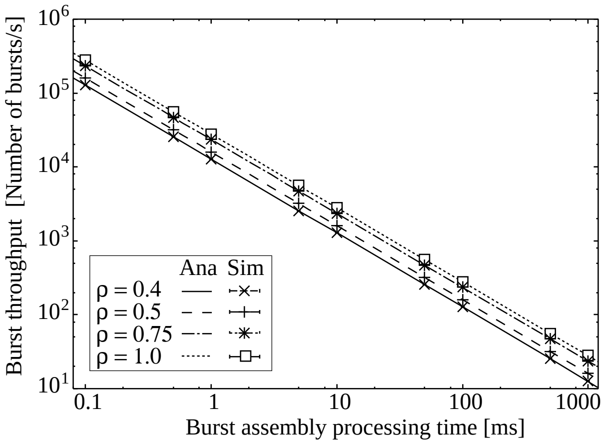


Fig. 10. Burst throughput vs. burst assembly processing time.

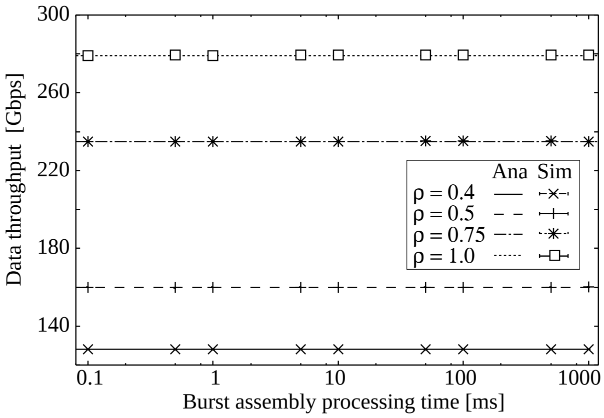


Fig. 11. Data throughput vs. burst assembly processing time.

### A.2 Impact of bursts from the other nodes

Next, we investigate how the bursts from the other nodes affect the performance of the timer-based burst assembly. Fig. 12 shows the relation between the arrival rate of bursts transmitted from the other nodes, $\lambda_o$, and the burst loss probability in the cases of $\lambda = 3.0$, 5.0, and 10.0. Figs. 13 and 14 show the results for the burst and data throughputs, respectively. Here, we set $W = 32$ and $T = 1.0$ ms.

From Fig. 12, we observe that the burst loss probability for the timer-based burst assembly increases as the arrival rate of bursts from the other nodes becomes large. This is simply because the system is overloaded. We also observe that the burst loss probability increases as the arrival rate of packets from the access network becomes large. This is due to the large bursts which are assembled with a number of IP packets at the edge node.

Comparing the loss probabilities for our analysis and the Erlang loss system in Fig. 12, the burst loss probability for the Erlang loss system is always larger than that for our analysis, while the results for our analysis is remarkably close to the simulation ones even when $\lambda_o$ is small. Note that the discrepancy between the Erlang loss system and simulation becomes large when $\lambda_o$ decreases.

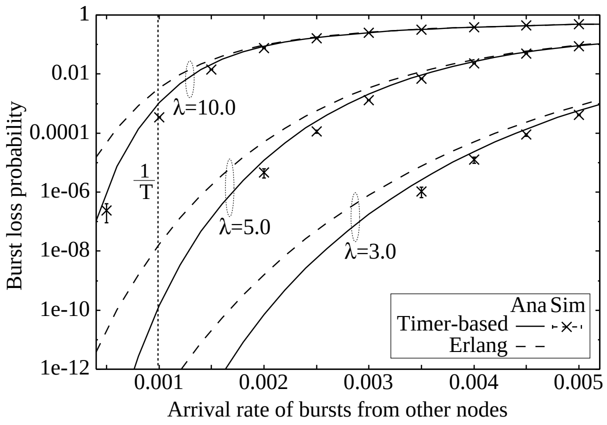


Fig. 12. Burst loss probability vs. arrival rate of bursts from other nodes.

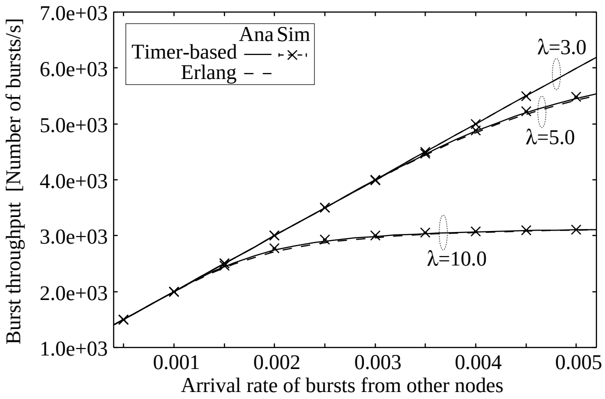


Fig. 13. Burst throughput vs. arrival rate of bursts from other nodes.

This implies that the accuracy of the Erlang loss system greatly depends on the arrival rate of the bursts from the other node and that our analytical model succeeds in predicting the burst loss probability in the case of small $\lambda_o$, where the Erlang loss model fails in providing the accurate value.

From Figs. 13 and 14, we observe that the burst and data throughputs become large and converge to constant values as the arrival rate of bursts from the other nodes increases. We also find that the burst throughput becomes small as the arrival rate of IP packets from the access network, $\lambda$, increases. This is because the burst size becomes large and this results in the increase of the burst loss probability. However, the number of packets assembled into a burst also increases and this causes large data throughput.

### A.3 Impact of the number of wavelengths

Fig. 15 shows how the number of wavelengths affects the loss probability for the timer-based burst assembly. In this figure, we set $\lambda = 10.0$ and $T = 1.0$ ms. The loss probabilities are calculated by the analysis and simulation in the cases of $\lambda_o = 0.001$, 0.002, 0.003 and 0.004. From this figure, we find again that the results of our analysis are close to the simulation results, while the results for the Erlang loss system are always larger than those for the simulation. On the other hand, the

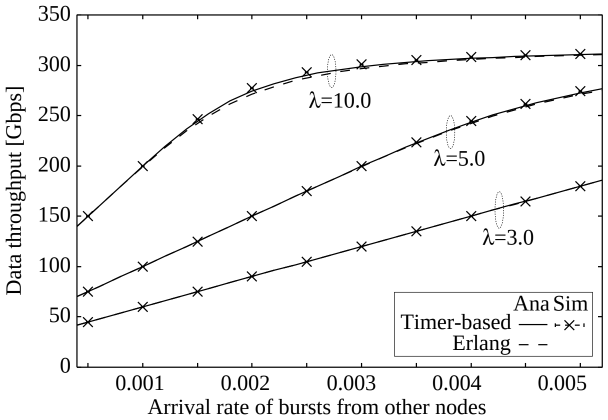


Fig. 14. Data throughput vs. arrival rate of bursts from other nodes.

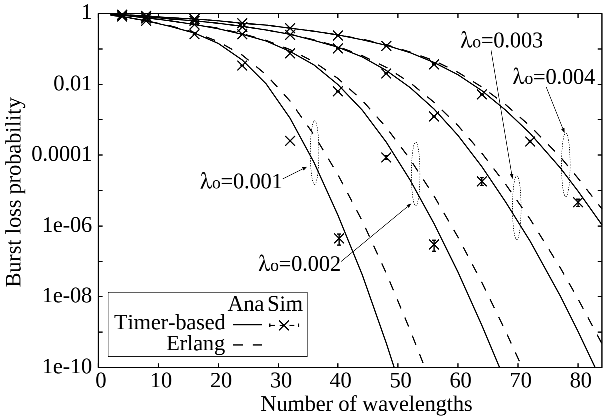


Fig. 15. Burst loss probability vs. number of wavelengths.

discrepancy among the analysis, Erlang loss model, and simulation becomes small as $W$ becomes large. Therefore, the Erlang loss model is useful for large $W$, however, our analysis is more useful than the Erlang loss model when the number of wavelengths is not large.

### *B. Ring network*

In this subsection, we investigate the effectiveness of our analysis for a uni-directional ring network. In the ring network with $L+1$ nodes, IP packets arrive at each node from its access network according to a Poisson process with rate $\lambda$ and the pair of source and destination nodes is uniformly distributed, i.e., any pair is selected with the same probability. In addition, we assume that the processing time of a control packet at each node is 1.0 ms and that the distance between each two nodes is 320 km. Here, the number of wavelengths is $W$ and the burst assembly time $T$ is equal to 1.0 [ms].

Table II illustrates the burst loss probability for our analysis, Erlang loss model, and simulation at an arbitrary link. Note that in the Geo,M/M/$W/W$ and Erlang loss models, we obtained the value of $\lambda_o$ from the simulation results in advance.

From this table, we can see the discrepancy between the analysis and simulation results. This

TABLE II
COMPARISON OF RESULTS OF GEO,M/M/$W/W$, ERLANG, AND SIMULATION IN UNI-DIRECTIONAL RING NETWORK.

| $(L+1, W)$ | $\lambda$ | Erlang | Geo,M/M/$W/W$ | Simulation |
|---|---|---|---|---|
| (5,8) | 3.0 | 1.77e-01 | 1.52e-01 | (6.24±0.96)e-02 |
| | 4.0 | 2.60e-01 | 2.36e-01 | (1.58±0.02)e-01 |
| (5,16) | 7.0 | 1.72e-01 | 1.53e-01 | (8.69±0.68)e-02 |
| | 8.0 | 2.15e-01 | 1.97e-01 | (1.38±0.02)e-01 |
| (10,16) | 3.5 | 1.34e-01 | 1.25e-01 | (6.54±0.54)e-02 |
| | 4.5 | 1.88e-01 | 1.78e-01 | (1.22±0.05)e-01 |
| (20,32) | 4.25 | 1.07e-01 | 1.03e-01 | (5.24±0.19)e-02 |
| | 8.0 | 2.00e-01 | 1.95e-01 | (1.60±0.01)e-01 |

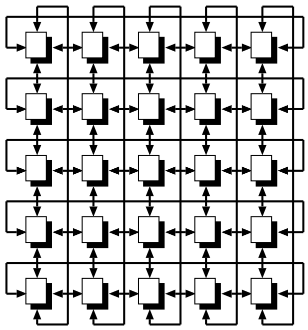

Fig. 16. Mesh-torus network with 25 nodes.

is because the burst arrival process from the other nodes is not a Poisson one in the simulation and the probability distribution of the resulting burst size is not an exponential one. However, the analysis result gives the upper bound of the simulation one and both results show the same tendency. As the numbers of nodes and wavelengths become large, our analysis result becomes close to the simulation one. Moreover in this table, we observe that our analysis can give the better estimate for the burst loss probability than the Erlang loss model. Hence, in the uni-directional ring network, our analytical model is useful for capturing the burst loss behavior in a qualitative sense.

### *C. Mesh-torus network*

Finally, we investigate the effectiveness of our analysis for a mesh-torus network with 25 nodes (see Fig. 16). We use the same parameters as those in the ring network. In this network, bursts are transmitted from source to destination nodes according to the deterministic routing algorithm as follows [9]. We define $D_x$ and $D_y$ as the shortest distance in the number of links from the destination node along the $x$ and y axes, respectively. When $D_x \geq D_y$ or $D_x = D_y < 2$, we choose a link on the $x$ axis as the next one to get closer to the destination node. When $D_x < D_y$ or $D_x = D_y = 2$, a link on the y axis is chosen. We repeat this procedure until $D_x$ and $D_y$ become zero. Here, each source node has 24 destination nodes and four output links. Note that according to the routing algorithm, each output link of the source node supports burst transmission to six

TABLE III
COMPARISON OF RESULTS OF GEO,M/M/$W$/$W$, ERLANG, AND SIMULATION IN MESH-TORUS NETWORK.

| $W$ | $\lambda$ | Erlang | Geo,M/M/$W$/$W$ | Simulation |
|---|---|---|---|---|
| 16 | 12.0 | 1.16e-01 | 1.08e-01 | (7.36±0.99)e-02 |
| | 15.0 | 1.60e-01 | 1.51e-01 | (1.47±0.13)e-01 |
| 32 | 26.0 | 7.99e-02 | 7.34e-01 | (5.92±0.68)e-02 |
| | 32.0 | 1.47e-01 | 1.40e-01 | (1.25±0.11)e-01 |

destination nodes. Each node has four pairs of burstifier and scheduler, and the cycle time of round-robin is 6.0 [ms] ($L = 6$ and $T$=1.0 [ms] in our analysis). We preobtained the value of $\lambda_o$ for the Geo,M/M/$W$/$W$ and Erlang loss models from the simulation results. In the following, we focus on any link in this network.

Table III illustrates the burst loss probability for the analysis, Erlang loss model, and simulation in the cases of $W = 16$ and 32. From this table, we observe the discrepancy between the analysis and simulation results, however, the discrepancy is smaller than that in the ring network. This is because each node in the mesh-torus network has more input and output links than that in the ring network, and the resulting burst arrival process is more close to a Poisson process. Moreover, our analysis gives the good estimate for the burst loss probability when the number of wavelengths is large and traffic load is heavy. From the above observation, our analytical model is useful for characterizing the burst loss behavior in the mesh-torus network.

## VI. CONCLUSIONS

In this paper, we considered the timer-based burst assembly with slotted scheduling for OBS networks. To evaluate its performance at an OBS edge node, we considered the Geo,M/M/$W$/$W$ model and explicitly derived the burst loss probability, burst throughput, and data throughput. Numerical examples showed that our analysis is efficient to evaluate the performance of the timer-based burst assembly in comparison with the Erlang loss system. In particular, our analysis is useful for the OBS network where a number of wavelengths are utilized and the arrival rate of bursts transmitted from other nodes is relatively small. Moreover, we observed that our analysis is also effective for large-scale uni-directional ring and mesh-torus networks with a large number of wavelengths.

## REFERENCES


[1] X. Cao, J. Li, Y. Chen, and C. Qiao, "Assembling TCP/IP Packets in Optical Burst Switched Networks," in *Proc. IEEE Globecom'02*, Nov. 2002, pp. 2808-2812.

[2] A. Detti and M. Listanti, "Impact of Segments Aggregation on TCP Reno Flows in Optical Burst Switching Networks," in *Proc. IEEE INFOCOM'02*, June 2002.

[3] K. Dolzer, "Assured Horizon - A New Combined Framework for Burst Assembly and Reservation in Optical Burst Switched Networks," in *Proc. NOC'02*, June 2002.

[4] K. Dolzer and C. Gauger, "On Burst Assembly in Optical Burst Switching Networks–A Performance Evaluation of Just-Enough-Time," in *Proc. 17th Int. Teletraffic Congress*, Sept. 2001, pp. 149-160.

[5] P. Fan, C. Feng, Y. Wang, and N. Ge, "Investigation of the Time-Offset Based QoS Support with Optical Burst Switching in WDM Networks," in *Proc. IEEE ICC'02*, May 2002, pp. 2682-2686.

[6] A. Ge and F. Callegati, "On Optical Burst Switching and Self-Similar Traffic," *IEEE Commun. Lett.*, vol. 4, no. 3, pp. 98-100, Mar. 2000.

[7] C. F. Hsu, T. L. Liu, and N. F. Huang, "Performance Analysis of Deflection Routing in Optical Burst-Switched Networks," in *Proc. IEEE INFOCOM'02*, June 2002.

[8] M. Izal and J. Aracil, "On the Influence of Self-Similarity in Optical Burst Switching Traffic," in *Proc. IEEE Globecom'02*, Nov. 2002, pp. 2308-2312.

[9] M. Kovačević and A. Acampora, "Benefits of Wavelength Translation in All-Optical Clear-Channel Networks," *IEEE J. Select. Areas Commun.,* vol. 14, no. 5, pp. 868-880, June 1996.

[10] H. Kröner, G. Hébuterne, P. Boyer, and A. Gravey, "Priority Management in ATM Switching Nodes," *IEEE J. Select. Areas Commun.*, vol. 9, no. 3, pp. 418-427, Apr. 1991.

[11] K. Long, R. S. Tucker, and C. Wang, "A New Framework and Burst Assembly for IP DiffServ over Optical Burst Switching Networks," in *Proc. IEEE Globecom'03*, Dec. 2003, pp. 3159-3164.

[12] X. Lu and B. L. Mark, "A New Performance Model of Optical Burst Switching with Fiber Delay Lines," in *Proc. IEEE ICC'03*, May 2003, pp. 1365-1369.

[13] D. Lucantoni, K. S. Meier-Hellstern, and M. F. Neuts, "A Single Server Queue with Server Vacations and a Class of Non-renewal Arrival Processes," *Adv. Appl. Probab.,* vol. 22, pp. 676-705, 1990.

[14] D. Morató, M. Izal, J. Aracil, E. Magaña, and J. Miqueleiz, "Blocking Time Analysis of OBS Routers with Arbitrary Burst Size Distribution," in *Proc. IEEE Globecom'03*, Dec. 2003, pp. 2488-2492.

[15] C. Qiao and M. Yoo, "Optical Burst Switching (OBS) - A New Paradigm for an Optical Internet," *J. High Speed Network*, vol. 8, no. 1, pp. 69-84, Jan. 1999.

[16] C. Qiao and M. Yoo, "Choices, Features and Issues in Optical Burst Switching," *Optical Net. Mag.*, vol. 1, no. 2, pp. 36-44, Apr. 2000.

[17] C. Qiao, "Labeled Optical Burst Switching for IP-over-WDM Integration," *IEEE Commun. Mag.*, vol. 38, no. 9, pp. 104-114, Sept. 2000.

[18] T. Tachibana, T. Ajima, and S. Kasahara, "Round-Robin Burst Assembly and Constant Transmission Scheduling for Optical Burst Switching Networks," in *Proc. IEEE Globecom'03*, Dec. 2003, pp. 2772-2776.

[19] J. Teng and G. N. Rouskas, "A Comparison of the JIT, JET, and Horizon Wavelength Reservation Schemes on A Single OBS Node," in *Proc. the First International Workshop on Optical Burst Switching*, Oct. 2003.

[20] V. M. Vokkarane, K. Haridoss, and J. P. Jue, "Threshold-based Burst Assembly Policies for QoS Support in Optical Burst-Switched Networks," in *Proc. SPIE OptiComm'02*, July 2002, pp. 125-136.

[21] V. M. Vokkarane, Q. Zhang, J. P. Jue, and B. Chen, "Generalized Burst Assembly and Scheduling Techniques for QoS Support in Optical Burst-Switched Networks," in *Proc. IEEE Globecom'02*, Nov. 2002.

[22] H. L. Vu and M. Zukerman, "Blocking Probability for Priority Classes in Optical Burst Switching Networks," *IEEE Commun. Lett.*, vol. 6, no. 5, pp. 214-216, May 2002.

[23] J. White, M. Zukerman, and H. L. Vu, "A Framework for Optical Burst Switching Network Design," *IEEE Commun. Lett.*, vol. 6, no. 6, pp. 268-270, June 2002.

[24] R. W. Wolff, *Stochastic Modeling and the Theory of Queues*. New Jersey: Prentice Hall, 1989.

[25] Y. Xiong, M. Vandenhoute, and H. C. Cankaya, "Control Architecture in Optical Burst-Switched WDM Networks," *IEEE J. Select. Areas Commun.*, vol. 18, no. 10, pp. 1838-1851, Oct. 2000.

[26] L. Yang, Y. Jiang, and S. Jiang, "A Probabilistic Preemptive Scheme for Providing Service Differentiation in OBS Networks," in *Proc. IEEE Globecom'03*, Dec. 2003, pp. 2689-2693.

[27] M. Yoo and C. Qiao, "Just-Enough-Time (JET): A High Speed Protocol for Bursty Traffic in Optical Networks," in *Proc. IEEE/LEOS Conf. on Technologies for a Global Information Infrastructure*, Aug. 1997, pp. 26-27.

[28] M. Yoo, C. Qiao, and S. Dixit, "QoS Performance of Optical Burst Switching in IP-Over-WDM Networks," *IEEE J. Select. Areas Commun.*, vol. 18, no. 10, pp. 2062-2071, Oct. 2000.

[29] X. Yu, Y. Chen and C. Qiao, "Study of Traffic Statistics of Assembled Burst Traffic in Optical Burst Switched Networks," in *Proc. Opticomm*, July 2002, pp. 149-159.